A CONSISTENT NONLINEAR SHELL ELEMENT BASED ON A COROTATIONAL FORMULATION FOR HYPERELASTIC MATERIAL MODELS

Ivan Moura Belo, ivanbelo@gmail.com
Marcelo Krajnc Alves, krajnc@emc.ufsc.br
Programa de Pós-Graduação em Engenharia Mecânica – POSMEC, Universidade Federal de Santa Catarina, Campus Universitário Trindade, Dep. Engenharia Mecânica - Bloco A, GMAC - Piso 2, CEP: 88.040-900, Florianópolis-SC, Brazil.

William Taylor Matias Silva, taylor@unb.br
Programa de Pós-Graduação em Estruturas e Construção Civil – PECC, Universidade de Brasília, Campus Darcy Ribeiro, Dep. Engenharia Civil e Ambiental, Edifício SG12 - 1º andar, CEP: 70.910-900, Brasília-DF, Brazil.

Abstract. *The corotational (CR) kinematic description is the most recent of the formulations proposed for geometrically nonlinear structural analysis. Because of this novelty, it has not reached the same level of maturity of the older Lagrangian formulations (Total and Updated). Much work remains to be done, particularly in material nonlinearities. Therefore, the aim of this paper is to develop an efficient shell element for hyperelastic analysis with two important assumptions: (i) strains from a corotated configuration are small while (ii) the magnitude of rotations from a base configuration is not restricted. The assumed natural deviatoric strain (ANDES) three nodes triangular shell element is implemented for hyperelastic material models and its application to different constitutive models is discussed. Results provided by the proposed shell element are compared with the results presented by other authors in the literature in order to show the adequacy of the presented theory and the effectiveness of the numerical procedure and shell element employed in this work.*

Keywords: *Geometrically nonlinear analysis, Corotational description, Shell finite elements.*

1. INTRODUCTION

In the last decades, the application of problems which are subjected to large displacements and rotations, but on the small strain domain increase. This covers important problems in several fields of the engineering because many structural materials can experience only fairly small strain, such as, aerospace structures, bridges, ships, automobiles motor-cars, sport material, etc.

In this context, the corotational (CR) kinematic description is viewed as an alternative way of deriving efficient nonlinear finite elements. The main idea of CR formulation is to decompose the motion of the element into rigid body and pure deformational parts, through the use of a reference system, which continuously rotates and translates with the element (Felippa, 1992). The term "corotational", also call "co-rotational" in the literature, relates here to the provision of a local system that continuously rotates and translates with the element, the definition of an element retraces to a change of variables from the local frame to the global one. This is done through the use of a projector matrix which relates the variations of the local displacements to the variations of the global ones, by extracting the rigid body modes from the latter.

The CR domain of application is limited by *a priori* kinematic assumptions, i. e., displacements and rotations may be arbitrarily large, but deformations must be small. Because of this restriction, corotational formulation has not penetrated the major general-purpose FEM codes that cater to nonlinear analysis. However, recent works provided by Felippa and co-workers, shows that the main interest of the corotational approach compared to the total Lagrangian (TL) one is that the transformation matrices are independent on the assumptions made for the local elements. This means that for elements with the same number of nodes and degrees of freedom, the corotational framework is the same. Consequently, many advantages of CR over TL description appears: (1) reuse of small-strain elements including materially nonlinear elements; (2) decouples small-strain material nonlinearities from geometric nonlinearities; (3) handles naturally the question of frame indifference of anisotropic behavior due to material nonlinearities (hyperelasticity, plasticity, creep). The rigid body transformation reorients automatically the material directions as long as strains remain small. This attribute eliminates the need to work with the cumbersome invariant stress rates of continuum mechanics and (4) is well suited to the treatment of structural elements with rotational degrees of freedom (beams, plates, shells) for arbitrarily large rotations. Such elements are notoriously difficult to treat with the TL description.

It is relevant to mention that because of the newness of CR description, many problems involving nonlinearities are unsolved. Materials for which the constitutive behavior is only a function of the current state of deformation are generally known as *elastic*. Under such conditions, any stress measure is a function of the current deformation gradient associated with that particle. However, in the special case when the work done by the stresses during a deformation process is

dependent only on the initial state at time t_0 and the final configuration at time t, the behavior of the material is said to be path-independent and the material is called *hyperelastic*.

A variety of efforts have been pursued over the past few decades to model the effective behavior of hyperelastic materials. Therefore, there are many hyperelastic constitutive models available in the literature. In order to explore the differences in their responses, the kinematic Consistent Simetrizable Equilibrated (CSE) corotational formulation and the Assumed Natural Deviatoric Strain (ANDES) three nodes triangular linear elastic shell finite element and the arch-length method joined with Newton-Raphson strategy (geometrically nonlinearity) are used. As an extension to acomodate the phisically nonlinearity (hyperelasticity), the material is assumed to be isotropic, incompressible Neo-Hookean hyperelastic solid.

2. COROTATIONAL FORMULATION

2.1 Shell element kinematics

The corotational description used in this work is fullly reviewed in many papers – Battini (1990), Pacoste and Felippa (1991), Felippa and Alexander (1992), Militello (1998), etc. For this reason, the CR kinematics used herein is briefly described. The key CR operation is to extract the deformational components of the translations and rotations for each node (Fig. 1), since the model is based on large displacements and rotation, however, in small-strain domain. Therefore, its is necessary to establish the deformational displacements vector in local frame ($\bar{\mathbf{v}}_d^e$), which stores the translational and rotational degrees of freedom for each node of the element:

$$\bar{\mathbf{v}}_d^e = \begin{bmatrix} \bar{\mathbf{v}}_{d1}^e & \cdots & \bar{\mathbf{v}}_{dN^e}^e \end{bmatrix}^T, \quad \text{with} \quad \bar{\mathbf{v}}_{da}^e = \begin{bmatrix} \bar{\mathbf{u}}_{da}^e \\ \bar{\boldsymbol{\theta}}_{da}^e \end{bmatrix}, \quad \text{for} \quad a = 1, \ldots, N^e \tag{1}$$

where a computes a nodal indice, N^e is the number of nodes in element e and the overbar represents that vector is based on local CR frame. In addition, $\bar{\mathbf{u}}_{da}^e$ and $\bar{\boldsymbol{\theta}}_{da}^e$ are the translational and rotational degrees of freedom of the element at node a, respectively.

In order to understand the key-concept of the corotational description, Fig. 1(a) shows a bar element moving in 2D space and how the total motion is separated. Figure 1(b) depicts a facet shell element, which moves from the initial position given by the position vector $\mathbf{r}^0$ to the deformed position given by the position vector $\mathbf{r}_d$.

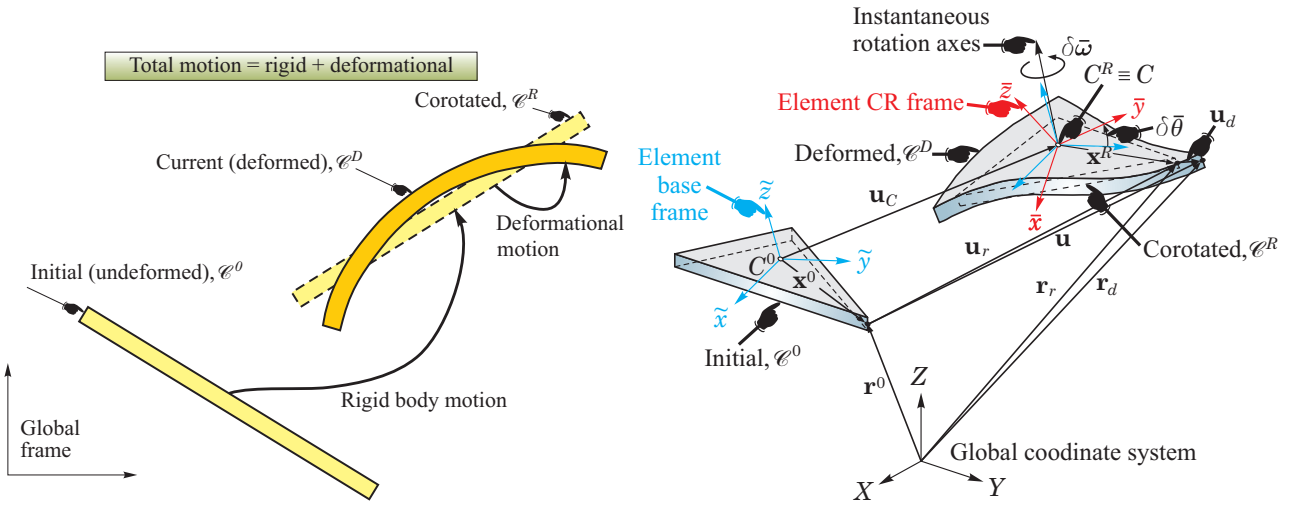

(a) Bar element moving in 2D space

(b) Facet shell element moving in 3D space

Figure 1. Basic concepts of the CR kinematic description, focusing on the separation of the total motion.

From the Fig. 1(b), the nodal displacements vector is computed from the initial configuration $\mathscr{C}^0$:

$$\mathbf{u} = \mathbf{r}_d - \mathbf{r}^0 \tag{2}$$

The displacement vector may be splits into rigid body displacement and deformational deformational as:

$$\mathbf{u} = \mathbf{u}_r + \mathbf{u}_d \tag{3}$$

The rigid body displacement $\mathbf{u}_r$ take place from initial $\mathscr{C}^0$ to corotated $\mathscr{C}^R$ configuration. The deformational displacement $\mathbf{u}_d$ is a vector joining points in $\mathscr{C}^R$ and $\mathscr{C}^D$. Taking into account geometrical considerations concerned to initial, corotated and current configurations and after tedious algebric manipulations, the vectors are calculated as follow:

$$\mathbf{u}_r = \mathbf{u}_C + (\mathbf{R} - \mathbf{I})\,\mathbf{x}^0 \quad \text{and} \quad \mathbf{u}_d = \mathbf{u} - \mathbf{u}_C - (\mathbf{R} - \mathbf{I})\,\mathbf{x}^0 \tag{4}$$

where $\mathbf{I}$ is the 3×3 identity matrix and $\mathbf{R}$ is the rotation tensor of a shell element node which is used to map the initial $\mathscr{C}^0$ to the final $\mathscr{C}^D$ configuration and it is given by:

$$\mathbf{R} = \mathbf{R}_d\mathbf{R}_0, \quad \text{with} \quad \mathbf{R}_0 = \mathbf{T}_R^T\mathbf{T}_0 \tag{5}$$

where $\mathbf{T}_0$ and $\mathbf{T}_R$ represent the linear transformation matrix from base element frame to global one and the element CR frame to global frame, respectively.

The rotation matrix $\mathbf{R}_d$ represents the deformational rotation and $\mathbf{R}_0$ is the rigid body rotation. Hence, this deformational spin may expressed in local CR frame as:

$$\bar{\mathbf{R}}_d = \mathbf{T}_R\mathbf{R}_d\mathbf{T}_R^T \tag{6}$$

The rotations in $\mathbb{R}^3$ are not commutative like they are in $\mathbb{R}^2$, because the in-plane rotation is defined by a scalar and the spatial rotation is described by both magnitude: the angle of rotation and its direction (Alvin *et al.*, 1992). For this reason, rotations in 3D space are sometimes pictured as vectors, however, finite 3D rotations do not obey the laws of vector calculus. The complete procedure to extract $\bar{\boldsymbol{\theta}}$ given by Eq. (1) of the $\mathbf{R}$ is demonstrated by Fellipa and Haugen (2005). Formally, this is $\bar{\boldsymbol{\theta}}_d = \text{Axial}\big[\log\left(\bar{\mathbf{R}}_d\right)\big]$. Finally, the vectors $\bar{\mathbf{u}}_d$ and $\bar{\boldsymbol{\theta}}_d$ are ready to be used in Eq. (1).

2.2 Degrees of freedom

The shell element used in this study is a triangular facet element shown in Fig. 2, with 18 degrees of freedom (6 per node: three rotations and three displacements). The displacements along the coordinate lines of a material point is defined by u_x, u_y and u_z. θ_x and θ_y are rotations of the normal about the $x-$ and $y-$ axes, respectively, and θ_z is the drilling degree of freedom introduced by Rankin and Brogan (1986). These DOFs are the same employed in Eq. (1).

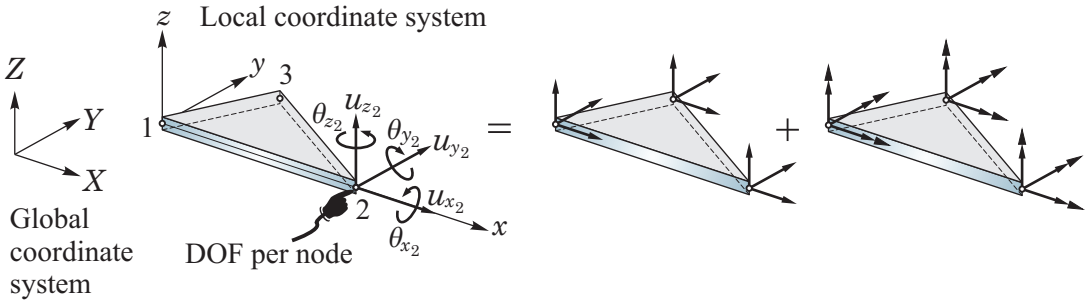

Figure 2. Node and freedom configuration of the facet shell triangle.

The geometry of the element is defined by the N^e coordinates $\mathbf{x}_a^0$, with $a = 1, \ldots, N^e$ at the initial configuration. The computation of the element centroid is done by simply averaging the coordinates of the element nodes, i. e.,

$$\mathbf{x}_{C^0}^e = \frac{1}{N^e}\sum_{a=1}^{N^e}\mathbf{x}_a^e \tag{7}$$

The algorithm to compute all displacements and rotations is given by Felippa and Haugen (2005).

2.3 Tangent stiffness matrix

The consistent tangent stiffness matrix $\mathbf{K}^e$ of element e is defined as the variation of the internal forces $\mathbf{p}^e$ with respect to element global freedoms $\mathbf{v}^e$:

$$\delta\mathbf{p}^e \overset{\text{def}}{=} \frac{\partial\mathbf{p}^e}{\partial\mathbf{v}^e}\delta\mathbf{v}^e = \mathbf{K}^e\delta\mathbf{v}^e \tag{8}$$

The element internal force vector $\mathbf{p}^e$ is given by Pacoste and Felippa (1991) and it is defined as the rate of the internal energy. This yields:

$$\mathbf{p}^e = \mathbf{T}^T\bar{\mathbf{P}}^T\bar{\mathbf{H}}^T\bar{\mathbf{p}}^e \tag{9}$$

where $\bar{\mathbf{P}}$ and $\bar{\mathbf{H}}$ are the projection operators. The first ensure the equilibrium of the internal force vector and the letter acts on the rotate degrees of freedom of the element in order to ensure symmetry of the consistent tangent stiffness matrix, for details about those matrix see Felippa (1992) and Cortivo (2009).

Cosidering Eqs. (8) and (9) give:

$$\delta\mathbf{p}^e = \overbrace{\delta\mathbf{T}^T\bar{\mathbf{P}}^T\bar{\mathbf{H}}^T\bar{\mathbf{p}}^e}^{1^{\text{st}}\text{ term}} + \overbrace{\mathbf{T}^T\delta\bar{\mathbf{P}}^T\bar{\mathbf{H}}^T\bar{\mathbf{p}}^e}^{2^{\text{nd}}\text{ term}} + \overbrace{\mathbf{T}^T\bar{\mathbf{P}}^T\delta\bar{\mathbf{H}}^T\bar{\mathbf{p}}^e}^{3^{\text{rd}}\text{ term}} + \overbrace{\mathbf{T}^T\bar{\mathbf{P}}^T\bar{\mathbf{H}}^T\delta\bar{\mathbf{p}}^e}^{4^{\text{th}}\text{ term}} \tag{10}$$

Now, the superscript $(\cdot)^e$, which represents the local frame, is going to be omitted and comparing Eqs. (8), (9) and (10) the consistent tangent stiffness matrix obtained by CR formulation is:

$$\mathbf{K} = \mathbf{K}_{GR} + \mathbf{K}_{GP} + \mathbf{K}_{GM} + \mathbf{K}_M \tag{11}$$

where $\mathbf{K}_{GR}$ is the rotational geometric stiffness, which represents the gradient of the internal force vector with respect to the rigid rotation of the element; $\mathbf{K}_{GP}$ is the equilibrium projection geometric stiffness, which expresses the variation of the projection of the internal force vector as the element geometry changes; $\mathbf{K}_{GM}$ is the moment correction geometric stiffness, which is generated by the variation of the Jacobian $\mathbf{H}$; and $\mathbf{K}_M$ is the material stiffness of the element, which expresses the variation of the element internal forces.

The completely procedure to obtain these matrix is described in Felippa and Haugen (2005). In this paper, their are just defined as:

$$\mathbf{K}_{GR} = -\mathbf{T}^T\bar{\mathbf{F}}_{nm}\bar{\mathbf{G}}\mathbf{T}, \quad \mathbf{K}_{GP} = -\mathbf{T}^T\bar{\mathbf{G}}^T\bar{\mathbf{F}}_n\bar{\mathbf{P}}\mathbf{T}, \quad \mathbf{K}_{GM} = \mathbf{T}^T\bar{\mathbf{P}}^T\bar{\mathbf{L}}\bar{\mathbf{P}}\mathbf{T}, \quad \mathbf{K}_M = \mathbf{T}^T\bar{\mathbf{P}}^T\bar{\mathbf{H}}^T\bar{\mathbf{K}}^e\bar{\mathbf{H}}\bar{\mathbf{P}}\mathbf{T} \tag{12}$$

where $\bar{\mathbf{F}}_{nm}$ and $\bar{\mathbf{F}}_n$ are the skew-symmetric spin matrices relative to axial forces $\bar{\mathbf{n}}$ and bending moments $\bar{\mathbf{m}}$ at node 1 and so on, respectively, and they are given by

$$\bar{\mathbf{F}}_{nm} = \begin{bmatrix} \text{Spin}\,(\delta\bar{\mathbf{n}}_1^e) \\ \text{Spin}\,(\delta\bar{\mathbf{m}}_1^e) \\ \vdots \\ \text{Spin}\,(\delta\bar{\mathbf{n}}_{N^e}^e) \\ \text{Spin}\,(\delta\bar{\mathbf{m}}_{N^e}^e) \end{bmatrix} \quad \text{and} \quad \bar{\mathbf{F}}_n = \begin{bmatrix} \text{Spin}\,(\delta\bar{\mathbf{n}}_1^e) \\ \vdots \\ \text{Spin}\,(\delta\bar{\mathbf{n}}_{N^e}^e) \end{bmatrix} \tag{13}$$

In addition, the matrix $\bar{\mathbf{G}}$ connects the variation in rigid element spin to the incremental translations and spins at the nodes, both with respect to the CR frame and can be written according Felippa and Haugen (2005) as:

$$\bar{\mathbf{G}} = \frac{1}{2A}\begin{bmatrix} 0 & 0 & x_{32}^C & 0 & 0 & 0 & 0 & 0 & x_{13}^C & 0 & 0 & 0 & 0 & 0 & x_{21}^C & 0 & 0 & 0 \\ 0 & 0 & y_{32}^C & 0 & 0 & 0 & 0 & 0 & y_{13}^C & 0 & 0 & 0 & 0 & 0 & 0 & 0 & 0 & 0 \\ 0 & \frac{-2A}{L_3} & 0 & 0 & 0 & 0 & 0 & \frac{2A}{L_3} & 0 & 0 & 0 & 0 & 0 & 0 & 0 & 0 & 0 & 0 \end{bmatrix}_{3\times 18} \tag{14}$$

where A is the triangle area, and L_3 is the length of side $\overline{12}$ of the triangle.

Also, the $\bar{\mathbf{K}}$ is the material linear elastic tangent stiffness matrix of the element and according to the ANDES formulation results:

$$\bar{\mathbf{K}} = \mathbf{K}_b + \mathbf{K}_h \tag{15}$$

Here $\mathbf{K}_b$ and $\mathbf{K}_h$ are called *basic* and *higher-order* stiffness matrices, respectively. $\mathbf{K}_b$ is formulation independent in that it is entirely defined by an assumed constant stress together with an assumed boundary displacement field and it is given by:

$$\mathbf{K}_b = \frac{1}{A}\mathbf{L}\mathbf{C}\mathbf{L}^T \tag{16}$$

where A is the shell element area, $\mathbf{C}$ is the stress-strain constitutive matrix and $\mathbf{L}$ is the matrix which has the deformational field of the element, and also is responsible for the stress lumping at nodes of the element. For brevity, this matrix can be found in Felippa and Haugen (2005).

$\mathbf{K}_h$ can be formed using several different formulations, in this work it will be use the Assumed Natural Deviatoric Strains (ANDES) formulation. The procedure for constructing the higher-order stiffness can be found in several sources as:

$$\mathbf{K}_h = \int_A \mathbf{B}_d^T\mathbf{C}\mathbf{B}_d\,dA \tag{17}$$

where $\mathbf{B}_d$ represents the deviatoric curvatures or deviatoric extensions. Thus, substituting (16) and (17) into (15) yields:

$$\bar{\mathbf{K}} = \frac{1}{A}\mathbf{L}\mathbf{C}\mathbf{L}^T + \int_A \mathbf{B}_d^T\mathbf{C}\mathbf{B}_d\,dA \tag{18}$$

3. HYPERELASTIC FORMULATION

3.1 Preliminary concepts

There are many hyperelastic constitutive models available in the literature, in this paper the model showed by Simo and Hughes (1998) is used. Let $\mathcal{B} \subset \mathbb{R}^3$ be the reference configuration of the body of interest. Assuming that $\mathcal{B}$ is open and bounded with smooth boundary $\partial\mathcal{B}$ and closure $\bar{\mathcal{B}} := \mathcal{B} \cup \partial\mathcal{B}$. Let [0, T] $\subset \mathbb{R}_+$ be the time interval of interest, and let $\mathbf{u} : \bar{\mathcal{B}} \times$ [0, T] $\rightarrow \mathbb{R}^3$ be the displacement field of particles with reference position $\mathbf{x} \in \mathcal{B}$ at time $t \in$ [0, T]. The infinitesimal strain tensor in terms of the displacement field is given by:

$$\boldsymbol{\varepsilon} = \frac{1}{2}\left[\nabla\mathbf{u} + (\nabla\mathbf{u})^T\right] = \frac{1}{2}\left(u_{i,j} + u_{j,i}\right)\mathbf{e}_i \otimes \mathbf{e}_j \tag{19}$$

where $\otimes$ denotes a tensor product. Second-order symmetric tensors are linear transformations in $\mathbb{S}$, defined as

$$\mathbb{S} := \left\{\boldsymbol{\xi} : \mathbb{R}^3 \rightarrow \mathbb{R}^3 | \boldsymbol{\xi} \text{ is linear, and } \boldsymbol{\xi} = \boldsymbol{\xi}^T\right\} \tag{20a}$$

This is a vector space with inner product,

$$\boldsymbol{\xi} : \boldsymbol{\xi} = \text{tr}(\boldsymbol{\xi}^T\boldsymbol{\xi}) \equiv \xi_{ij}\xi_{ij} \tag{20b}$$

where tr$(\cdot)$ is the trace of the tensor into parenthesis, which is defined as the sum of the diagonal components.

The simplest model for a constitutive equation is provided by a hyperelastic material, for which the stress response is characterized in terms of a stored energy function $W : \mathcal{B} \times \mathbb{S} \rightarrow \mathbb{R}$, such that:

$$\boldsymbol{\sigma}(\mathbf{x}) = \frac{\partial W\left[\mathbf{x}, \boldsymbol{\varepsilon}(\mathbf{x})\right]}{\partial \boldsymbol{\varepsilon}} \tag{21}$$

which is an expression of the stress tensor. This tensor can be written in function of the constitutive material behavior as:

$$\boldsymbol{\sigma} = \boldsymbol{\mathcal{C}}\boldsymbol{\varepsilon}, \quad \text{with} \quad \boldsymbol{\mathcal{C}} = \frac{\partial^2 W\left[\mathbf{x}, \boldsymbol{\varepsilon}(\mathbf{x})\right]}{\partial \boldsymbol{\varepsilon}^2}, \quad \text{in components: } \mathcal{C}_{ijkl} = \frac{\partial^2 W}{\partial\varepsilon_{ij}\partial\varepsilon_{kl}} \tag{22}$$

Remark 1. *It is assumed that $\boldsymbol{\mathcal{C}}$ is positive-definite restrict to $\mathbb{S}$ and symmetric, i. e., $\mathcal{C}_{ijkl} = \mathcal{C}_{klij} = \mathcal{C}_{ijlk} = \mathcal{C}_{jilk}$.*

3.2 Frame indifference

Recalling that the constitutive equation for a hyperelastic material is defined in terms of a stored-energy function which depends on the deformation locally only through the deformation gradient, that is, a function $W[\mathbf{x}, \mathbf{F}(\mathbf{x}, t)]$ is given such that,

$$\mathbf{P}(\mathbf{x}, t) = 2\mathbf{F}\frac{\partial W}{\partial \mathbf{C}}, \quad \mathbf{S} = 2\frac{\partial W}{\partial \mathbf{C}} \quad \text{and} \quad \boldsymbol{\tau} = 2\mathbf{F}\frac{\partial W}{\partial \mathbf{C}}\mathbf{F}^T \tag{23}$$

where $\mathbf{P}$ and $\mathbf{S}$ represent the first and the second Piola–Kirchhoff stress tensor, respectively; $\mathbf{F}$ is the deformation gradient, which is the derivative of the deformation; $\mathbf{C}$ is the right Cauchy-Green deformation tensor, which is given by $\mathbf{C} = \mathbf{F}^T\mathbf{F}$; and $\boldsymbol{\tau}$ is the Kirchhoff stress tensor. Therefore, the stored-energy function $W(\mathbf{x}, \mathbf{F})$ is said to be objective or frame indifferent.

3.3 Isotropic hyperelasticity

Isotropy is defined by requiring the constitutive behavior to be identical in any material direction. This implies that the relationship between strain energy W and $\boldsymbol{\mathcal{C}}$ must be independent of the material axes chosen and, consequently, W must only be a function of the invariants of $\mathbf{C}$ as:

$$I_1 := \text{tr}(\mathbf{C}) = \sum_{i=1}^{3} C_{ii} = C_{11} + C_{22} + C_{33} \tag{24a}$$

$$I_2 := \frac{1}{2}\left[I_1^2 - \text{tr}(\mathbf{C}^2)\right] = \sum_{i=1}^{3} C_{ii}^2 = C_{11}^2 + C_{22}^2 + C_{33}^2 \tag{24b}$$

$$I_3 := \det(\mathbf{C}) = \prod_{i=1}^{3} C_{ii} = C_{11}C_{22}C_{33} \tag{24c}$$

where the components C_{ii} are precisely derived from the eigenvalues problem. Now, using the following relationships:

$$\frac{\partial I_1}{\partial \mathbf{C}} = \mathbf{I}, \quad \frac{\partial I_2}{\partial \mathbf{C}} = I_1\mathbf{I} - \mathbf{C} \quad \text{and} \quad \frac{\partial I_3}{\partial \mathbf{C}} = I_3\mathbf{C}^{-1} \tag{25}$$

and the constitutive Eqs. (23), the symmetric Piola–Kirchhoff tensor becomes:

$$\mathbf{S} = 2\left(\frac{\partial W}{\partial I_1} + \frac{\partial W}{\partial I_2}I_1\right)\mathbf{I} - 2\frac{\partial W}{\partial I_2}\mathbf{C} + 2\frac{\partial W}{\partial I_3}I_3\mathbf{C}^{-1} \tag{26}$$

Using the relation $\boldsymbol{\tau} = \mathbf{F}\mathbf{S}\mathbf{F}^T$, the following constitutive equation for the Kirchhoff stress is obtained,

$$\boldsymbol{\tau} = 2\left(\frac{\partial W}{\partial I_3}I_3\right)\mathbf{I} + 2\left(\frac{\partial W}{\partial I_1} + \frac{\partial W}{\partial I_2}I_1\right)\mathbf{b} - 2\frac{\partial W}{\partial I_2}\mathbf{b}^2 \tag{27}$$

where $\mathbf{b} = \mathbf{F}\mathbf{F}^T$ is the left Cauchy-Green deformation tensor.

3.4 The hyperelastic CR approach

Consistent with the assumption of isotropy and the notion of an intermediate stress-free configuration, the stress response by a stored-energy function is characterized by:

$$W = U(J^e) + \bar{W}(\bar{\mathbf{b}}^e), \quad \text{with} \quad \bar{\mathbf{b}}^e := J^{e^{-\frac{2}{3}}}\mathbf{F}^e\mathbf{F}^{e^T} \equiv J^{e^{-\frac{2}{3}}}\mathbf{b}^e \tag{28}$$

where $U : \mathbb{R}_+ \to \mathbb{R}_+ \cup \{0\}$ is a convex function of $J := \det(\mathbf{F}^e)$ and the volumetric and deviatoric parts of W are represented by $U(J^e)$ and $\bar{W}(\bar{\mathbf{b}}^e)$, respectively, and their relations are defined as:

$$U(J^e) := \frac{1}{2}\kappa\left[\frac{1}{2}\left(J^{e^2} - 1\right) - \log_{\mathbf{e}} J^e\right] \quad \text{and} \quad \bar{W}(\bar{\mathbf{b}}^e) := \frac{1}{2}\mu\left[\text{tr}\left(\bar{\mathbf{b}}^e\right) - 3\right] \tag{29}$$

where $\mu > 0$ and $\kappa > 0$ are interpreted as the shear and bulk modulus, respectively. The definition of $\bar{\mathbf{b}}^e$ yields $\det(\bar{\mathbf{b}}^e) = 1$, hence, the denomination of the deviatoric part assigned to $\bar{W}$. Also,

$$\text{tr}(\bar{\mathbf{b}}^e) = \text{tr}(\bar{\mathbf{C}}^e), \quad \text{where} \quad \bar{\mathbf{C}}^e := J^{e^{-\frac{2}{3}}}\mathbf{F}^{e^T}\mathbf{F}^e \tag{30}$$

Finally, let $W = U(J^e) + \hat{W}(\bar{\mathbf{C}}^e)$ and comparing (28) and (30), $\bar{W}(\bar{\mathbf{b}}^e) = \hat{W}(\bar{\mathbf{C}}^e)$. Then the Kirchhoff stress tensor is obtained by the general expression:

$$\boldsymbol{\tau} = 2\mathbf{F}^e\frac{\partial W}{\partial \mathbf{C}^e}\mathbf{F}^{e^T} = J^eU'(J^e)\mathbf{I} + \mathbf{s}, \quad \text{where} \quad \mathbf{s} = 2\,\text{dev}\left(\bar{\mathbf{F}}^e\frac{\partial \hat{W}}{\partial \bar{\mathbf{C}}^e}\bar{\mathbf{F}}^{e^T}\right) \tag{31}$$

where dev$(\cdot)$ denotes the deviatoric part of $(\cdot)$. Note that the uncoupled, stored-energy function (28) results in uncoupled volumetric-deviatoric stress-strain relationships, which is very important to CR approach. From the Eqs. (30) and (29),

$$\boldsymbol{\tau} = J^e p\mathbf{I} + \mathbf{s} \tag{32a}$$

$$p := U'(J^e) = \frac{\kappa\left(J^{e^2} - 1\right)}{2J^e} \tag{32b}$$

$$\mathbf{s} := \text{dev}(\boldsymbol{\tau}) = \mu\,\text{dev}(\bar{\mathbf{b}}^e) \tag{32c}$$

Note that $U(J) \to +\infty$ and $p \to \pm\infty$, as $J \to 0$ and $J \to \infty$. Further, it can easily show that Eq. (32) reduces, for small strains, to the classical isotropic model of the linearized theory. In the computational context, the hyperelastic constitutive model (32) evaluated at time t_{n+1} yields:

$$\boldsymbol{\tau}_{n+1} = J^e_{n+1}p_{n+1}\mathbf{I} + \mathbf{s}_{n+1} \tag{33a}$$

$$p_{n+1} := U'(J^e_{n+1}) \tag{33b}$$

$$\mathbf{s}_{n+1} := \mu\,\text{dev}(\bar{\mathbf{b}}^e_{n+1}) \tag{33c}$$

This is a main part of the the full algorithm described in Simo and Hughes (1998) with porpose to abridge this paper.

4. NUMERICAL STUDIES

In order to examinate the response from the considered hyperelatic model, a set of numerical comparison between the hyperelastic model presented in the literature and the model described in the preceding section is performed. The objective is to provide a set of simple yet representative test problems with well established numerical results. The important restriction of the CR formulation showed through this paper is in the fact that the displacements and rotations are large, although the strains are small. Thus, the hyperelastic model presented in this paper regards this limitation.

4.1 A simple patch test

The first example is a simple plane-stress tension test (see Fig. 3). The problem consists of a square hyperelastic plate under two axial concentrated loads applied at the free corners. The mechanical properties and dimensions of the plate are the following: Young's modulus $E = 1.0 \times 10^6$; Poisson's ratio $\nu = 0.3$; side $L = 10.0$ and side-to-thickness ratio $L/h = 10$. Figure 3(b) shows the simple mesh implemented in order to avaliate the model.

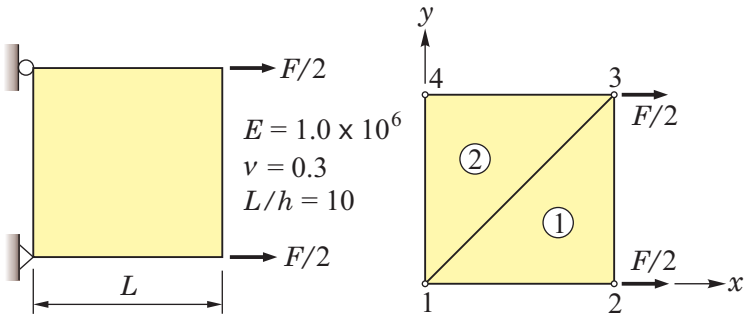

(a) Problem description (b) Analyses descretization

Figure 3. A simple plane stress axial test.

To solve a system of nonlinear algebric equations, different strategies is employed, such as the cylindrical arc-lenght method, the normal plane method of Riks-Wempner and the updated normal plane method of Ramm. All these three strategies were combined with the full Newton-Raphson method in order to control progress along the equilibrium path. Therefore, the iteration process is continued until the difference between the update configuration and the previous one reduces to a preselected error tolerance, which is $\epsilon \leqslant 10^{-6}$, is adopted and results are obtained using 20 load steps for this first application.

Remark 2. *For details of the strategies used to solve the nonlinear system, see Haugen (1994).*

Figure 4 depicts the gradual development of the axial displacement with the load increase. The continuous line represents the deformed configuration at each load step.

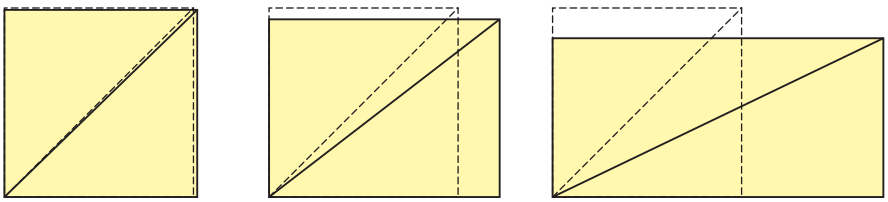

Figure 4. Deformed configuration through analyses.

The finite element solution is compared with Toscano and Dvorkin (2007) and Fig. 5 clearly shows very good agreement of the model proposed. To the first load step, for example, the axial displacement obtained by Toscano and Dvorkin (2007) was 0.16 while the CR hyperelastic element gives 0.12, i. e., a percentual difference of the 0.75%. To the last load step, this diffefence increase to 0.998%.

4.2 Cantilever under constant moment

The next example is described in Fig. 6. The initially-straight cantilever is clamped at one end (all displacements zero) and loaded by a constant moment M at the other end. The analytical solution corresponds to a beam rolled up into a

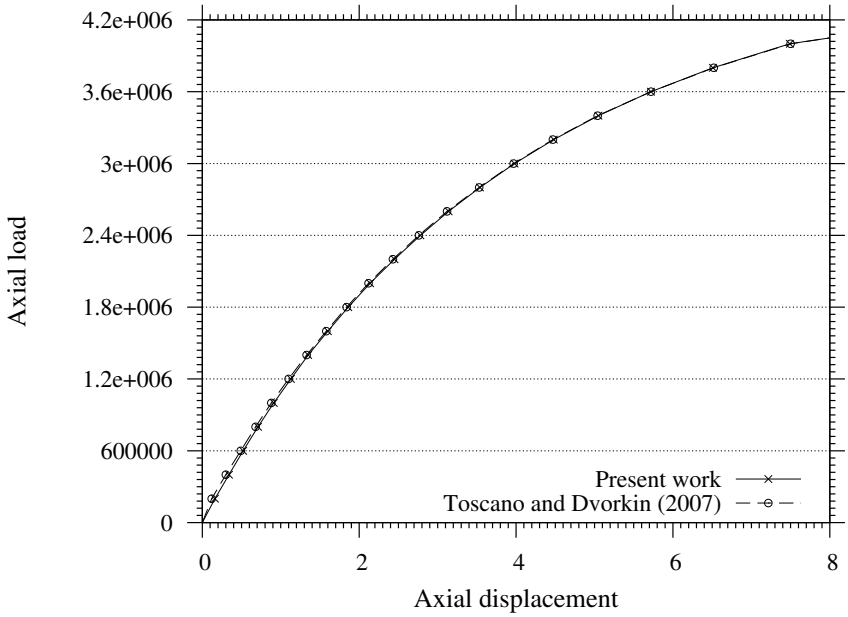

Figure 5. Axial displacement at the node 2.

circular arc of radius R given by:

$$\frac{1}{R} = \frac{M}{EI} \tag{34}$$

In order to test the singularity-free nature of the present element, it is investigated the case in which the beam rolled up into a complete circle ($\theta = 2\pi$) using a mesh of 20 elements. This example does not test the full three-dimensional behaviour but, in two-dimensions, is a severe test of inextensional bending. The material and geometrical properties are choosen as $E = 1.2 \times 10^7$, $L/b = 10$, $L/h = 100$ and $\nu = 0$.

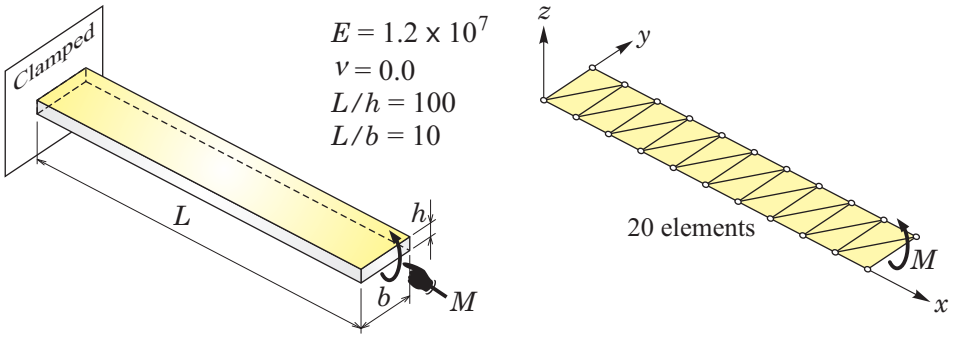

Figure 6. Initial geometry for cantilever subject-to-end moment and the discretization of the problem.

The analysis is performed using 20 elements with uniform 10×1 mesh. The solution is obtained using six equal steps of $\Delta M = \frac{M}{6}$. At each step, convergence was achieved to $\epsilon \leqslant 10^{-4}$ in three iterations. Figure 7 depicts all steps of the analyses and the rotation versus moment applied. Compared to the analytical solution, the element CR formulation underpredicts rotations by 1.32% while the element proposed in Toscano and Dvorkin (2007) overpredicts by about 1.84%. Hence, the present element displays better results then other element, although this difference was very small.

Remark 3. *In this example, the applied nodal moment load is choosen because it is non-conservative. The "standard" corotational formulations are usually not able to solve problems with non-conservative loads, but the element proposed is in excellent agreement with the solution obtained by Toscano and Dvorkin (2007) and the analitycal solution.*

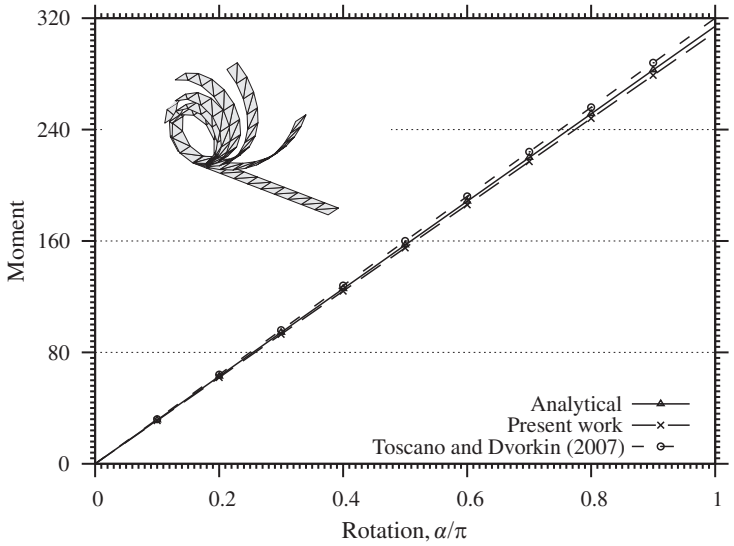

Figure 7. Initial and deformed geometries for cantilever under constant moment and the convergence of the solutions.

4.3 Hemispherical isotropic shell

The next case shown in Fig. 8 refers to the pinched hemispherical shell with a 18° hole. The loads are two pairs of inward and outward point loads, 90° apart. This analysis is used as a test case in many previous publications because its highly warped shell problem. To give good results for these problems, two properties must be demonstrated by the CR hyperelastic shell element: an inextensional-bending mode must be allowed and secondly, a rigid body motion must be well expressed. For symmetry reasons, the problem is modeled using only one quarter of the hemisphere. The material properties are $E = 6.825 \times 10^7$ and $\nu = 0.3$, the radius is $R = 10$ and the thickness is $h = 0.04$.

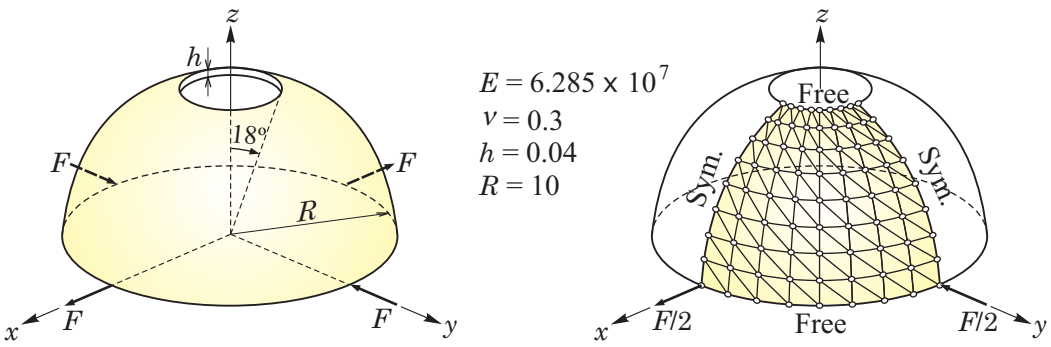

Figure 8. Pinched hemispherical shell with a 18° hole.

The problem is solved using three uniform meshes; namely, 4×4, 8×8 and 16×16 with 32, 128 and 512 elements, respectively. The plot of a pinching load values versus the displecement under the corresponding applied load is shown in Fig. 9. The three top curves correspond to the displacements under y direction, while the lower curves represent the displacements under x axis, see Fig. 9(a). The results obtained using either of the three meshes, are in excellent agreement with the results reported by Simo *et al*. (1990). In a poor mesh, the difference between present element and the element proposed by Toscano and Dvorkin (2007) is hardly noticeable. Figure 9(b) helps to demonstrate the behavior of the solutions.

Figure 10 shows the deformed mesh configuration (16×16) and this computation was carried out in 5 iterations. This represents a half of iterations obtained by Simo *et al.* (1990) for the same mesh.

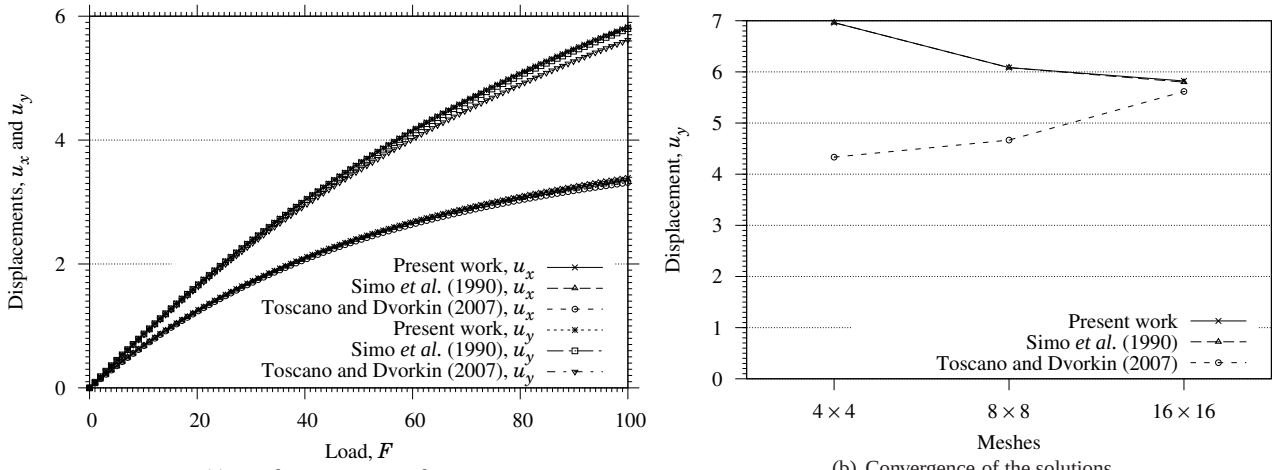

(a) Displacements u_x and u_y

(b) Convergence of the solutions

Figure 9. The displacement-load plots for the different models of the pinched hemisphere analysis.

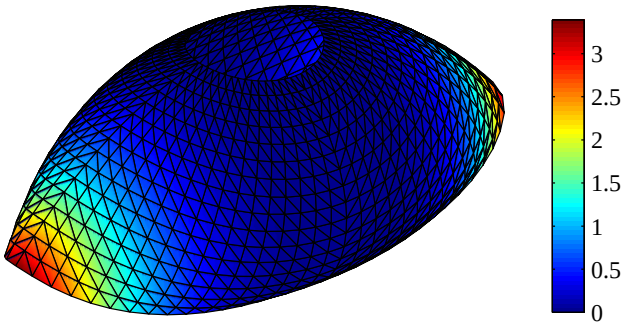

Figure 10. Nodal displecements of the 16×16 mesh, the value labeled in a right scale refers to the displacement u_x.

5. SUMMARY AND CONCLUSIONS

The paper has described the development of the corotational triangular shell element for hyperlastic materials. The ANDES approach found in the literature, has been used as local formulation. Three numerical applications have shown that the proposed element can be used to analyse problems presenting large displacements and rotations, but small strains. If this assumption is violated for a coarse discretization, it is necessary break it into more elements. For this reason, in the context of hyperelasticity, the model must be incompressible Neo-Hookean solid.

A excellent agreement with analytical and numerical results have been obtained with fine and coarse meshes, and also with distorted elements. It can be concluded that it is advantageous to use CR description because using the described corotational framework, efficient linear elements are automatically transformed to nonlinear formulations.

6. ACKNOWLEDGEMENTS

The authors would like to acknowledge CNPq for the scholarship provided to the first author of this paper.

7. REFERENCES

Alvin, K. *et al.*, 1992, "Membrane triangles with corner drilling freedoms–I. The EFF element", Finite Elements in Analysis and Design, Vol. 12, pp. 163 - 187.

Battini, J-M. *et al.*, 1990, "Improved minimal augmentation procedure for the direct computation of critical points", Comput. Methods Appl. Mech. Engrg., Vol. 81, pp. 131 - 150.

Cortivo, N. D. *et al.*, 2009, "Plastic buckling and collapse of thin shell structures, using layered plastic modeling and co-rotational ANDES finite elements", Comput. Methods Appl. Mech. Engrg., Vol. 198, pp. 785 - 798.

Felippa, C. A., 2006, "Supernatural QUAD4: A template formulation", Comput. Methods Appl. Mech. Engrg., Vol. 195,

pp. 5316 - 5342.
Felippa, C. A., 1994, "A survey of parametrized variational principles and applications to computational mechanics", Comput. Methods Appl. Mech. Engrg., Vol. 113, pp. 109 - 139.
Felippa, C. A. and Alexander, S., 1992, "Membrane triangles with corner drilling freedoms – III. Implementation and performance evaluation", Finite Elements in Analysis and Design, Vol. 12, pp. 203 - 239.
Felippa, C. A., 1992, "Membrane triangles with corner drilling freedoms – II. The ANDES element", Finite Elements in Analysis and Design, Vol. 12, pp. 189 - 201.
Felippa, C. A. and Haugen, B., 2005, "A unified formulation of small-strain corotational finite elements: I. Theory", Comput. Methods Appl. Mech. Engrg., Vol. 194, pp. 2285 - 2335.
Haugen, B., 1994, "Buckling and stability problems for thin shell structures using high performance finite elements", Ph.D thesis of University of Colorado, EUA.
Militello, C., 1998, "Co-rotational flat facet triangular elements for shell instability analyses", Comput. Methods Appl. Mech. Engrg., Vol. 156, pp. 75 - 110.
Pacoste, C. and Felippa, C. A., 1991, "The first ANDES elements: 9-dof plate bending triangles", Comput. Methods Appl. Mech. Engrg., Vol. 93, pp. 217 - 246.
Rankin, C. C. and Brogan, F. A., 1986. "An element-independent corotational procedure for the treatment of large rotations", ASME J. Pressure Vessel Technology, Vol. 108, pp. 165 - 174.
Simo, J. C. *et al.*, 1990. "On stress resultant geometrically exact shell model. Part III: computational aspects of the nonlinear theory", Comput. Meth. Appl. Mech. Eng., Vol. 73, pp. 53 - 92.
Simo, J. C. and Hughes, T. J. R., 1998, "Computational Inelasticity: Interdisciplinary Applied Mathematics", Vol. 7, Ed. Springer-Verlag New York, Inc., 404 p.
Toscano, R. G. and Dvorkin, E. N., 2007, "A shell element for finite strain analyses: hyperelastic material models", Int. J. Computer-Aided Engrg., Vol. 24, pp. 514 - 535.

8. RESPONSIBILITY NOTICE

The authors are the only responsible for the printed material included in this paper.